Actomyosin II contractility expels von Willebrand factor from Weibel–Palade bodies during exocytosis

Thomas D. Nightingale,[1,2,3] Ian J. White,[1,2] Emily L. Doyle,[1,2,3] Mark Turmaine,[3] Kimberly J. Harrison-Lavoie,[1,2,3] Kathleen F. Webb,[1,2] Louise P. Cramer,[1,3] and Daniel F. Cutler[1,2,3]

[1]Medical Research Council Laboratory for Molecular Cell Biology, [2]Cell Biology Unit, and [3]Department of Cell and Developmental Biology, University College London, London WC1E 6BT, England, UK

The study of actin in regulated exocytosis has a long history with many different results in numerous systems. A major limitation on identifying precise mechanisms has been the paucity of experimental systems in which actin function has been directly assessed alongside granule content release at distinct steps of exocytosis of a single secretory organelle with sufficient spatiotemporal resolution. Using dual-color confocal microscopy and correlative electron microscopy in human endothelial cells, we visually distinguished two sequential steps of secretagogue-stimulated exocytosis: fusion of individual secretory granules (Weibel–Palade bodies [WPBs]) and subsequent expulsion of von Willebrand factor (VWF) content. Based on our observations, we conclude that for fusion, WPBs are released from cellular sites of actin anchorage. However, once fused, a dynamic ring of actin filaments and myosin II forms around the granule, and actomyosin II contractility squeezes VWF content out into the extracellular environment. This study therefore demonstrates how discrete actin cytoskeleton functions within a single cellular system explain actin filament–based prevention and promotion of specific exocytic steps during regulated secretion.

Introduction

Regulated secretion is a fundamental cellular event, which is critical to normal physiology. Very many cells release premade bioactive proteins from storage organelles in response to external stimulation (Burgoyne and Morgan, 2003). The overall process of regulated secretion from assembly at the TGN to post-Golgi trafficking to final exocytosis and release of granule cargo comprises multiple stages. Exocytosis of mature organelles is itself extremely complex and has many different steps for an individual organelle (Burgoyne and Morgan, 2003).

A role for actin in the final secretory stages, i.e., in regulated exocytosis, has been studied for several decades with a long-recognized history of different outcomes reported in different cellular systems (Cingolani and Goda, 2008; Trifaró et al., 2008). Actin has been reported to function in two broad ways: to prevent or, paradoxically, to promote exocytosis. One of the oldest ideas for a preventative role is that in several cell types, actin filaments within the cell cortex (Cramer, 1999a) function as a physical barrier to prevent exocytosis (Doreian et al., 2008; Berberian et al., 2009; Bittins et al., 2009; Deng et al., 2009). Another, not mutually exclusive, view is that in endothelial and other cells, a separate population of actin filament bundles (sometimes termed stress fibers) located within the cell cytoplasm (Cramer, 1999a) forms protein–protein structural links with secretory organelles to directly anchor them (Desnos et al., 2003; Waselle et al., 2003; Hume et al., 2007; Nightingale et al., 2009), which is a very different role to a physical barrier function.

Earlier bodies of work on actin function largely assessed regulated secretion at a cell population or tissue level. Relatively recent investigations have imaged actin at the single or cluster of granule level (Valentijn et al., 2000b; Sokac et al., 2003, 2006; Nemoto et al., 2004; Yu and Bement, 2007; Bhat and Thorn, 2009; Miklavc et al., 2009). Actin filaments are associated with several different types of exocytic organelles, mainly appearing as a ring or coat on the organelle membrane

L.P. Cramer and D.F. Cutler contributed equally to this paper.

Correspondence to Daniel F. Cutler: d.cutler@ucl.ac.uk

Abbreviations used in this paper: CCE, cytochalasin E; HUVEC, human umbilical vein endothelial cell; TEM, transmission EM; VWF, von Willebrand factor; WPB, Weibel–Palade body.

The Rockefeller University Press $30.00
J. Cell Biol. Vol. 194 No. 4 613–629
www.jcb.org/cgi/doi/10.1083/jcb.201011119

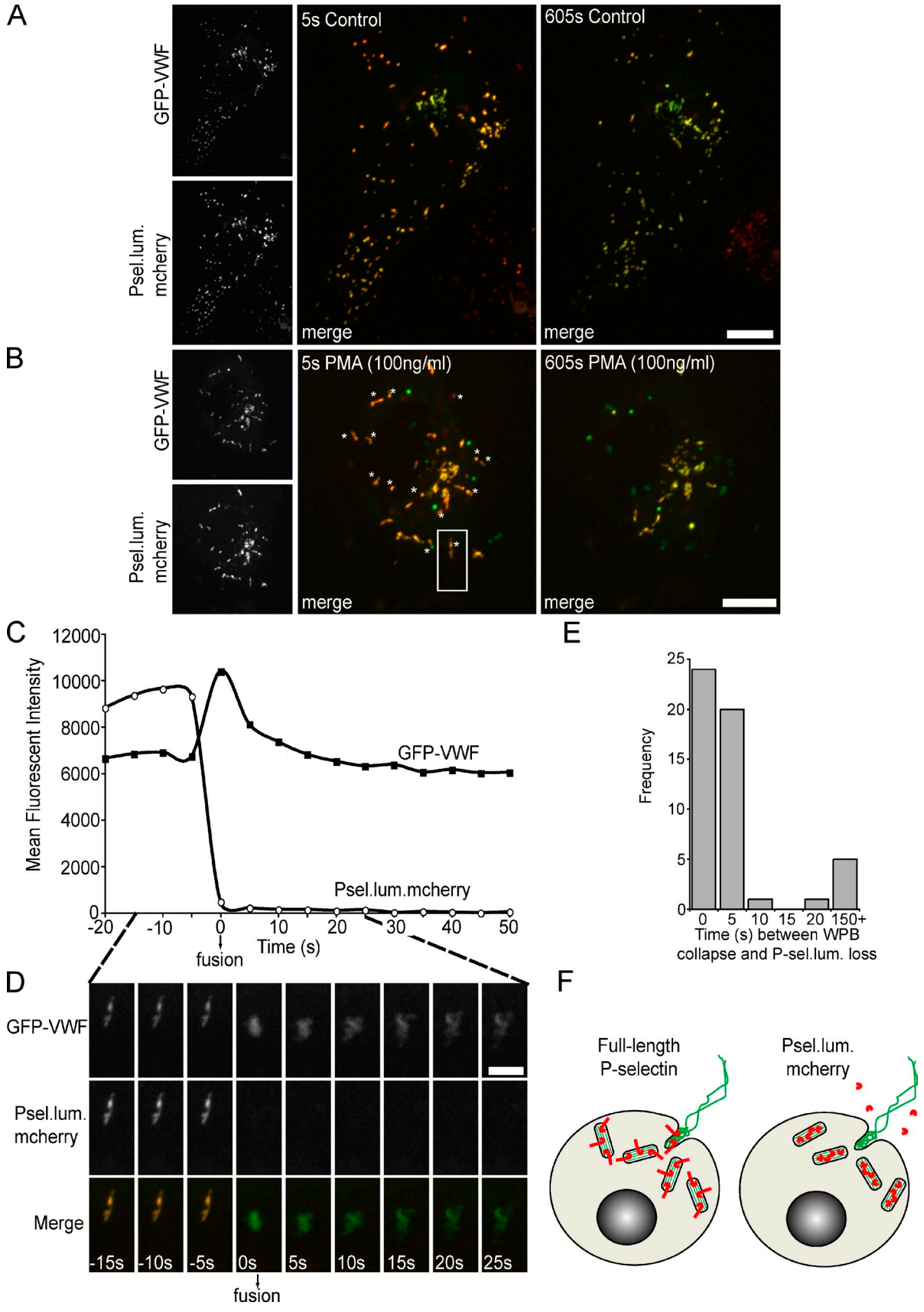

Figure 1. **Spinning-disk confocal microscope assay for monitoring fusion of—and VWF release from—individual WPBs in live cells.** (A–E) HUVECs were nucleofected with the mCherry–P-selectinLum domain and GFP-VWF and imaged with a spinning-disk confocal microscope system in the absence (A) or presence (B–E) of 100 ng/ml PMA. Time on the panels indicates total time in media (A), media with PMA (B), or relative to fusion (0 s; C–E). Z stacks were

(Bhat and Thorn, 2009). From these more recent observations, both positive and negative regulations have been inferred, involving various mechanistic functions. Actin filament coats might prevent exocytosis by slowing down fusion of the organelle with the plasma membrane (Nemoto et al., 2004). In converse, it is envisaged that the coats speed up exocytosis by helping the organelle move to the plasma membrane before fusion (Valentijn et al., 2000a). Postfusion actin filaments and myosin II may work together to maintain an open exocytic pore (Larina et al., 2007; Berberian et al., 2009; Bhat and Thorn, 2009), to provide a contractile force to expel granule content (Schietroma et al., 2007; Miklavc et al., 2009), or once cargo has been secreted, to retrieve granule membranes during compensatory endocytosis (Sokac et al., 2003, 2006).

Although all of these hypotheses are potentially attractive, no one experimental system has directly visualized and distinguished the fusion event together with the release of content step after fusion; in most cases, it is only known whether the fusion pore is open, which does not directly report cargo release. A similar problem is that actin dynamics have not been directly correlated with the exit of cargo from fused organelles. Hence, identification of precise actin-based mechanisms for fusion and for exit of cargo events after fusion for any one system remains difficult. Furthermore, one obvious implication of results such as these is that actin might prevent exocytosis before fusion yet augment it after fusion within a single secretory cell system. This is consistent with work titrating actin inhibitors (Gasman et al., 2004; Mitchell et al., 2008) yet has not yet been explicitly and directly tested within a single secretory cell system.

We wished to directly test roles of actin for both the fusion and the release of cargo steps. We have therefore analyzed actin function at these two discrete steps of exocytosis in a single organellar system, monitoring release of endogenous and physiologically relevant cargo. To do this, we chose Weibel–Palade bodies (WPBs), the regulated secretory organelles of endothelial cells (Weibel and Palade, 1964; Metcalf et al., 2008).

WPBs are involved in the initiation and control of inflammatory, hemostatic, angiogenic, and other vascular phenomena (Sadler, 2008). Their size and shape are driven by the presence of von Willebrand factor (VWF; Wagner et al., 1991; Michaux et al., 2006a), a 220-kD glycoprotein that dimerizes in the ER and begins to multimerize at the TGN after propeptide cleavage. The multimers then bind the propeptide again to rearrange into proteinaceous tubules that run parallel to the long axis of the organelle, causing its unique elongated shape (Wagner, 1990; Sadler, 2009). At exocytosis, the intraorganellar pH of 5.5 rises to neutrality (Erent et al., 2007b), and the propeptide is released, allowing the orderly unfurling of VWF into the flowing plasma as millimeter-long protein strings that act to recruit platelets to form a hemostatic plug (Dong et al., 2002). WPB cargo also includes the type 1 membrane protein leukocyte receptor P-selectin (Bonfanti et al., 1989; McEver et al., 1989), which is recruited into forming WPBs by the binding of its luminal domain to VWF (Michaux et al., 2006b). At exocytosis, P-selectin rapidly diffuses away from the site of organelle fusion (Babich et al., 2008), whereas VWF cargo is released much more slowly from the same WPB (Babich et al., 2008). Thus, these two proteins provide ideal probes for monitoring different stages of exocytosis. Furthermore, the low number of granules per cell, the large size of the organelles (≤5 µm long), and their relatively slow exocytosis together provide an ideal opportunity for light microscopy to be used in examining the role of actin at different stages of exocytosis by probing single secretory organelles.

WPBs are anchored by Rab27A and its effectors to actin filament bundles within the cytoplasm (Nightingale et al., 2009) to prevent premature exocytosis. We now propose that after secretagogue has triggered release from these tethers to allow exocytic fusion, a highly dynamic actomyosin II filament ring associated with the organelle then functions to expel VWF outwards. Thus, actin filaments both prevent and augment the exocytosis of a single regulated secretory organelle.

Results

A two-color assay of different stages of the exocytosis of individual WPBs

Different stages of exocytosis of WPBs are easily monitored because P-selectin moves away from exocytic sites at fusion, whereas release of VWF into the extracellular environment occurs later (Babich et al., 2008). To use P-selectin as a selective monitor for the early exocytic event of fusion, we expressed its soluble luminal WPB-targeting domain tagged with mCherry (termed mCherry–P-selectinLum). The removal of transmembrane and cytoplasmic domains prevents its reentry into endocytic and recycling routes. This provides a functional readout for fusion by monitoring the disappearance of the mCherry signal. Other markers of fusion (Erent et al., 2007a) that rely on specific behaviors of VWF and GFP were also used (see paragraph after next for details). To follow postfusion events,

acquired at a spacing of 0.5 µm every 5 s for 10 min, and images shown represent maximum intensity projections. (A, unstimulated) mCherry–P-selectinLum (Psel.lum.mcherry) and GFP-VWF are colocalized in WPBs, and there is a similar number of WPBs 605 s later. Individual WPBs move within the cytoplasm over time. Smaller images show individual channels of the 5-s merged image. (B, PMA stimulated) mCherry–P-selectinLum and GFP-VWF remain colocalized within WPBs by 5 s of PMA stimulation. Smaller images show individual channels of the 5-s merged image. By 605 s, many WPBs have exocytosed (asterisks indicate WPBs that fully exocytose during the time course of imaging). (C) Quantification of the intensity of fluorescence of mCherry–P-selectinLum and GFP-VWF for the individual organelle shown in D. Note that decrease in mCherry–P-selectinLum fluorescence (−5 to 0 s) occurs before the decrease in GFP-VWF fluorescence (−5 to 25 s) in the same WPB. (D) Still images of a video of exocytosis of the WPB in the box in B. The WPB becomes rounded in shape (compare GFP-VWF at −5 and 0 s), and this is linked to loss of mCherry fluorescence intensity (compare −5 and 0 s). (E) Quantification of the interval between formation of a rounded GFP-VWF shape and loss of mCherry fluorescence intensity for the population of exocytosing WPBs at 5-s time resolution (plotted from 51 events in five cells). (F) Schematic of exocytosis of full-length P-selectin and the P-selectin luminal domain. Bars: (A and B) 10 µm; (D) 4 µm.

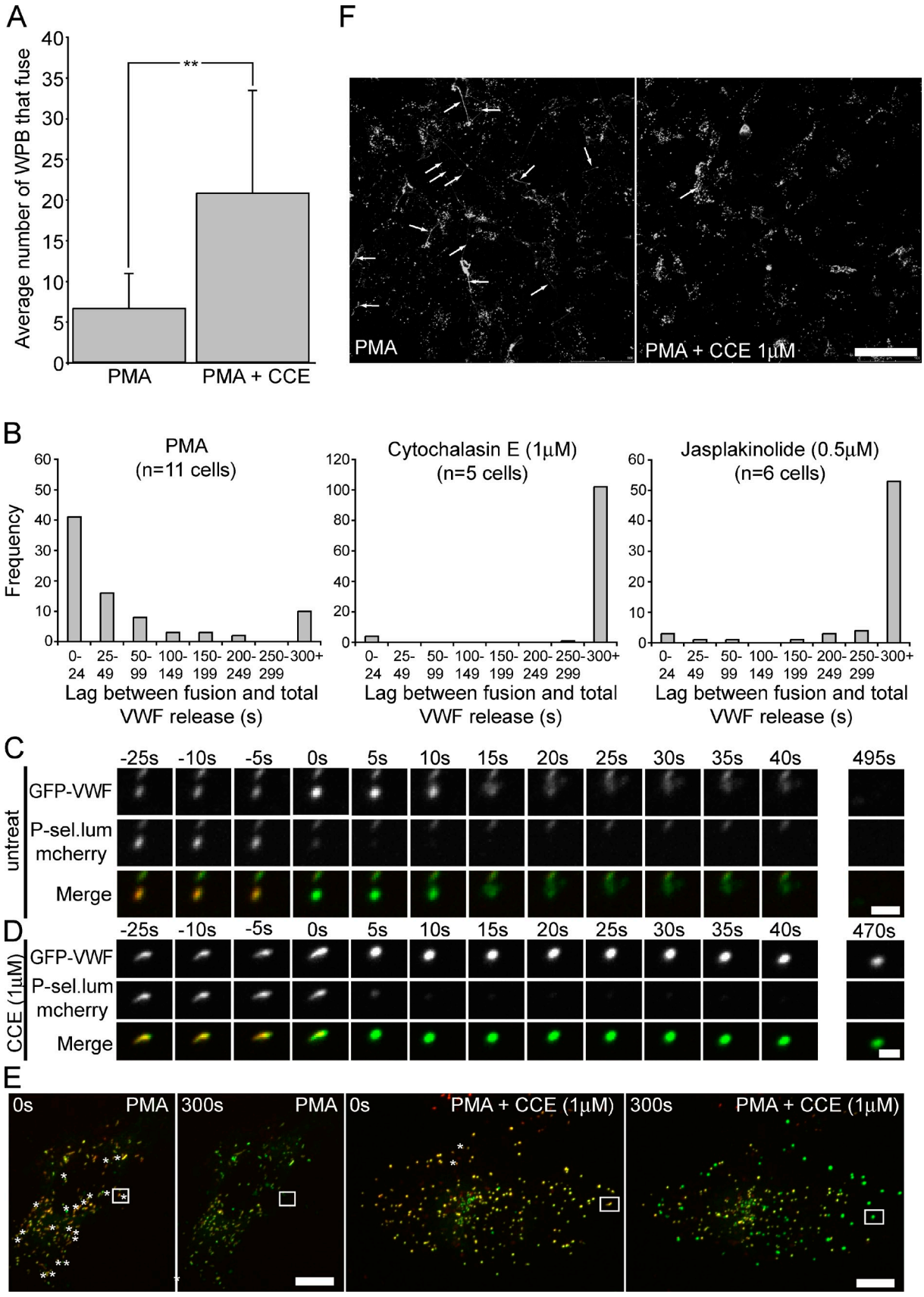

Figure 2. **Effect of CCE on WPB exocytosis.** (A, B, D, and E) HUVECs coexpressing GFP-VWF and the mCherry–P-selectinLum domain were stimulated with 100 ng/ml PMA for 10 min with or without a 15-min preincubation with 1 µM CCE (A, B, D, and E) or 0.5 µM jasplakinolide (B). Individual WPB fusion events (marked by loss of mCherry–P-selectinLum [P-sel.lum.mcherry] fluorescence) and release of its GFP-VWF contents (marked by loss of GFP fluorescence

VWF internally tagged with GFP (GFP-VWF) provides a well-characterized, well-behaved chimera to track the slow secretion of the granule core content. Transiently coexpressed mCherry–P-selectinLum and GFP-VWF allowed direct observation of individual WPB exocytosis throughout the whole endothelial cell using spinning-disk confocal microscopy at high temporal and spatial resolution (see Live-cell imaging; Fig. 1).

In the absence of a secretagogue, both fluorescence markers are localized within individual WPBs in cells, and the numbers of WPBs do not change with time, though granules move within the cytoplasm (Fig. 1 A and Video 1). In response to the secretagogue (PMA), the proportion of labeled WPBs decreases as granules exocytose (Fig. 1 B). The mCherry signal is lost first, whereas the GFP-VWF signal initially remains within the same individual organelle (Fig. 1, C and D; and Video 2).

The loss of mCherry–P-selectinLum fluorescence intensity correlates with two other fusion-related events. Upon fusion, there is a morphological change from a cigar-shaped to a more "collapsed," rounded WPB-shaped structure (Fig. 1 D, compare −5 and 0 s), as the rise in pH that occurs upon fusion also allows unfurling of the tightly coiled VWF that controls WPB shape. Furthermore, there is a transient rapid rise in GFP-VWF fluorescence intensity (Fig. 1, C and D, 0 s) also caused by increased pH upon fusion, correlating with the opening of a fusion pore (Erent et al., 2007a). At a 5-s time resolution, rapid loss of mCherry fluorescence into bathing medium is tightly linked to both these other markers of fusion. For most WPBs, mCherry fluorescence disappears at the same time as (0 s) or within 5 s of formation of round-shaped WPBs (Fig. 1, D and E) and is coincident with the transient rise in brightness of the GFP-VWF signal (Fig. 1, C and D, compare −5 and 0 s from still images and trace). A minority of WPBs become rounded but fail to lose mCherry (∼10%; Fig. 1 E); these are likely undergoing lingering kiss exocytosis whereby a smaller pore forms, allowing release of only small cargo content (Babich et al., 2008). Such events are excluded from our dataset as mCherry–P-selectinLum is too big to exit. At a 5-s time resolution, fusion identified with these three markers typically takes 0–5 s.

Total release of VWF is often well separated from and takes longer than the granule fusion event. We assessed WPB fusion (loss of mCherry–P-selectinLum fluorescence) and total secretion of VWF (complete loss of GFP-VWF fluorescence) with a 5-s temporal resolution. For the majority of events, the lag between granule fusion and mean total time to release VWF is 21.7 s (70/84), varying between 5 and 70 s for individual organelles. For the remaining minority of 14 organelles, 4/14 take 100–200 s, and 10/14 take 300+ s. Within a single cell, exocytosis is asynchronous; individual WPBs initiate exocytosis at any point during 10 min of continuous stimulation, consistent with the biochemical measurement of VWF secretion (Michaux et al., 2006a). For comparisons of different individual WPBs, we normalized the fusion step to 0 s (Fig. 1, C and D). We conclude that rapid decrease in mCherry–P-selectinLum fluorescence is a faithful readout of the fusion of individual WPBs with the plasma membrane, whereas slower loss of GFP-VWF fluorescence reflects subsequent release of contents from the same individual organelle.

The effect of actin poisons on different stages of individual WPB exocytosis

We next treated cells with cytochalasin E (CCE) to inhibit actin filament assembly. We chose conditions (15 min with 1 µM CCE) to target both stable and dynamic actin structures. Cortical actin filaments and stress fibers with which WPBs are associated are relatively stable with a half-life of 10–25 min. This CCE treatment causes an ∼50% reduction in stress fibers in human umbilical vein endothelial cells (HUVECs) with no detectable change in cell shape or cell adhesion, suggesting that there is no major disruption to general cell organization (Nightingale et al., 2009).

Consistent with actin filaments anchoring granules in endothelial cells (Nightingale et al., 2009), CCE causes an increase in WPB motility (Manneville et al., 2003) and an increase in fusion events (Fig. 2 A), i.e., events in which disappearance of mCherry–P-selectinLum fluorescence and conversion to round-shaped GFP-VWF structures occurred from the same double-labeled WPB after secretagogue addition. In stark contrast, GFP-VWF release from fused WPBs is blocked within CCE-treated cells (Fig. 2, B and compare C and D; and Video 3). The duration of release was quantified by determining the interval between fusion and complete loss of GFP-VWF signal (Fig. 2 B). In 95.3% (102/107) of cases, the duration of VWF release is >300 s, significantly longer than controls, and most WPBs had still not released contents by the end of the video (600 s of filming) or in cases in which we imaged cells for 30 min. We obtained similar data when assaying VWF release by ELISA (Nightingale et al., 2009). These CCE-treated WPBs cease exocytosis at fusion, as indicated by the prolonged duration of round GFP-VWF–positive structures (Fig. 2 D). Stills from low

into the medium) in live cells were assayed as described in Fig. 1. To compare individual WPBs, fusion is assigned to 0 s (see Results for explanation). (A) Mean number of individual WPB fusion events in 300 s (n = 11 cells for each condition). Note a more than threefold increase in fusion events in CCE-treated, PMA-stimulated cells. **, P = 0.004; t test. Error bars show SDs. (B) Duration of release of VWF measured as the lag between WPB fusion and full release of GFP-VWF for individual WPBs in live PMA-stimulated cells (83 fusion events in 11 cells) or in PMA-stimulated cells treated with CCE (107 fusion events in five cells) or jasplakinolide (66 fusion events from six cells). 300+ s indicates that VWF failed to release during 600 s of time-lapse filming. (C, control) Still images from a video of individual WPB fusion and release of VWF in live cells. (D, CCE treated) Note that in CCE-treated cells, WPB fusion occurs (0 s), yet GFP-VWF fails to release even after 470 s after fusion. (E) Whole-cell view of untreated or CCE-treated, PMA-stimulated live cells. Asterisks indicate WPBs that fully exocytose during 300 s of imaging. The boxed regions are the regions shown at higher magnification in C and D at a number of time points. Images shown (C–E) represent maximum intensity projections of z stacks. (F) Cells were fixed and labeled for released VWF. Note that markedly less VWF strings are apparent in CCE-treated compared with untreated, PMA-stimulated cells. The arrows denote the presence of the strings of VWF. Bars: (C and D) 2 µm; (E) 10 µm; (F) 100 µm.

power videos show that a CCE-treated cell simply accumulates a set of interrupted exocytic events (Fig. 2 E), and platelet-catching VWF strings on the surface of secretagogue-stimulated HUVECs are also absent (Fig. 2 F). Pretreating cells with jasplakinolide to block actin filament disassembly (Cramer, 1999b) similarly blocks release of VWF contents (Fig. 2 B), suggesting that dynamic actin filaments are required for the late stage of exocytosis.

Actin filaments are rapidly recruited to exocytosing WPBs

To support our data suggesting that dynamic actin filaments promote the release of VWF, we used Lifeact (Riedl et al., 2008), an actin filament–binding peptide, coupled to a red or green fluorophore to monitor actin filament behavior. Cells co-transfected with Lifeact plus either mCherry–P-selectinLum or GFP-VWF and then stimulated with secretagogue (Fig. 3) show that actin ring–type structures are visibly and rapidly recruited to 78% of exocytosing WPBs (Fig. 3, A–C; and Video 4). The minority of 22% may be below the limit of detection for our system. This actin filament ring appears exceptionally dynamic with a total lifetime ranging 10–32 s in individual WPBs (Fig. 3 D). Careful analysis shows that actin ring formation usually occurs after fusion of WPBs (Fig. 3, B, C, and E–G). In most cases (26/39), ring formation and decay (10–32 s; Fig. 3 D) are approximately coincident with the timing of total release of GFP-VWF (5–49 s; Fig. 2 B, PMA), and the two events are often simultaneous or near simultaneous when assayed together for an individual fused organelle (Fig. 3, C and G). In a minority of cases (10/39), actin recruitment cannot be temporally resolved from fusion (Fig. 3 E), but again, the ring lasts until the final release of GFP-VWF. These data are consistent with a direct and active role for dynamic actin filaments in the later stages of exocytosis of WPBs, i.e., secretion of granule core content.

Higher resolution imaging within fixed cells, of three secretory events (Fig. 4, A and B) viewed in xyz sections, shows that the actin filaments are located as a ring at or near the bottom of the granule (Fig. 4, C and D). Time-lapse microscopy assessing vertical sections during exocytosis of single fused WPBs shows that the granule moves relative to the plasma membrane, whereas the associated actin filament ring remains stationary toward the plasma membrane distal end of the WPB (Fig. 5 and Video 5), consistent with the actin ring driving movement of the fused granule toward the plasma membrane to effect content extrusion.

Myosin II activity is required for VWF release from fused organelles

Nonmuscle myosin II might be involved in exocytosis (Andzelm et al., 2007; Doreian et al., 2008; Berberian et al., 2009; Bhat and Thorn, 2009), and HUVECs express the IIB isoform (Fig. 6 B). We examined the localization of myosin II at exocytosis and found that it localized to the actin ring (Fig. 6 A). Both actin filaments (Fig. 3 and Fig. 5) and myosin II (Fig. 6 A) localize to fused organelles and are not obviously enriched on WPBs yet to fuse. Treating HUVECs with 25 µM (−)-blebbistatin (active enantiomer), a specific inhibitor of myosin II (Straight et al., 2003), has no effect on WPB fusion (Fig. 6 C), but release of VWF as measured by ELISA is reduced more than twofold (Fig. 6 D). When assessing fusion visually, it is apparent that WPB release of VWF is defective; VWF remains within WPBs >95 s after fusion (Fig. 6 E) compared with a mean of 21.7 s in untreated cells (Fig. 3). Analysis of Lifeact-Ruby by spinning-disk microscopy (Fig. 6, E–H) shows that the total lifetime of the actin filament ring increases about threefold, ranging from 20 to 60 s (Fig. 6 E-G) in blebbistatin-treated cells compared with 10–30 s in controls (Fig. 3 D), and the proportion of exocytosing WPBs to which actin is recruited is reduced by ∼1.5-fold (Fig. 6 H compared with Fig. 3 A). Thus, for secretion of VWF content, actin filaments (Fig. 2) and myosin II (Fig. 6) are similarly required.

We then wished to analyze in more detail the observed myosin II–dependent release of VWF (Fig. 6, D and E) from fused WPBs by exploiting the two-color assay (Fig. 1). For our experimental system, this would require the use of blue light in the presence of blebbistatin. In vitro, blue light blocks blebbistatin activity (Sakamoto et al., 2005). However, in cells, the effect is unclear; some studies report that activity is similarly inhibited (Sakamoto et al., 2005; Charras et al., 2006), whereas in other cellular systems, blebbistatin clearly remains active in the presence of blue light (Murthy and Wadsworth, 2005). We tested the effect of blue light on blebbistatin activity for WPB exocytosis and found that, as shown for cytokinesis in epithelial cells (Murthy and Wadsworth, 2005), blebbistatin remains active. We found no difference in the total lifetime of the actin filament ring in the presence of blebbistatin with (mean of 38.9 s; Fig. S3, A–C) or without (mean of 36.3 s; Fig. 6, E–G) blue light compared with blebbistatin-untreated cells (mean of 18.3 s; Fig. 3). Similarly, blue light had no detectable effect on the blebbistatin-induced effects on actin recruitment to WPBs (compare Fig. S3 D [with blue light] and Fig. 6 H [without blue light]). We agree with others that the difficulties in effectively blocking blebbistatin activity with blue light in cells might reflect constant diffusion of active drug into cells (Sakamoto et al., 2005) or depend on technical differences in imaging or cellular systems. Having established that blue light is unlikely a concern for VWF exocytosis, we assessed myosin II–based VWF exocytosis (Fig. 6, D and E) in more detail for individual granules in the two-color assay (Fig. S3 E). In blebbistatin-treated cells, in 64% (25/39) of fused granules, VWF release fails over the time course of imaging (Fig. S3 E, 300+ s), a time that is ∼10-fold longer than controls (Fig. 3 and Fig. S3 E). For the other 36% of fused WPBs, release of VWF is slower or similar to controls (Fig. S3 E).

We also blocked myosin II contractility by other methods. Specific inhibitors of myosin light chain kinase (Fig. 7, A and C–G) or Rho kinase (Fig. 7 B) similar to blebbistatin do not block fusion of WPBs (Fig. 7 C) yet do reduce VWF release from fused organelles (Fig. 7, A–C), with VWF failing to release from 70% of individual fused WPBs during 600 s of observation (Fig. 7 C). We also noted similar effects on recruitment of actin to fused WPBs (Fig. 7 G) and an increase in the total lifetime of the actin filament ring that formed (Fig. 7, D–F) in treated cells. Although the effect on lifetime in ML-7–treated cells was not as marked as that seen with blebbistatin, presumably other regulators

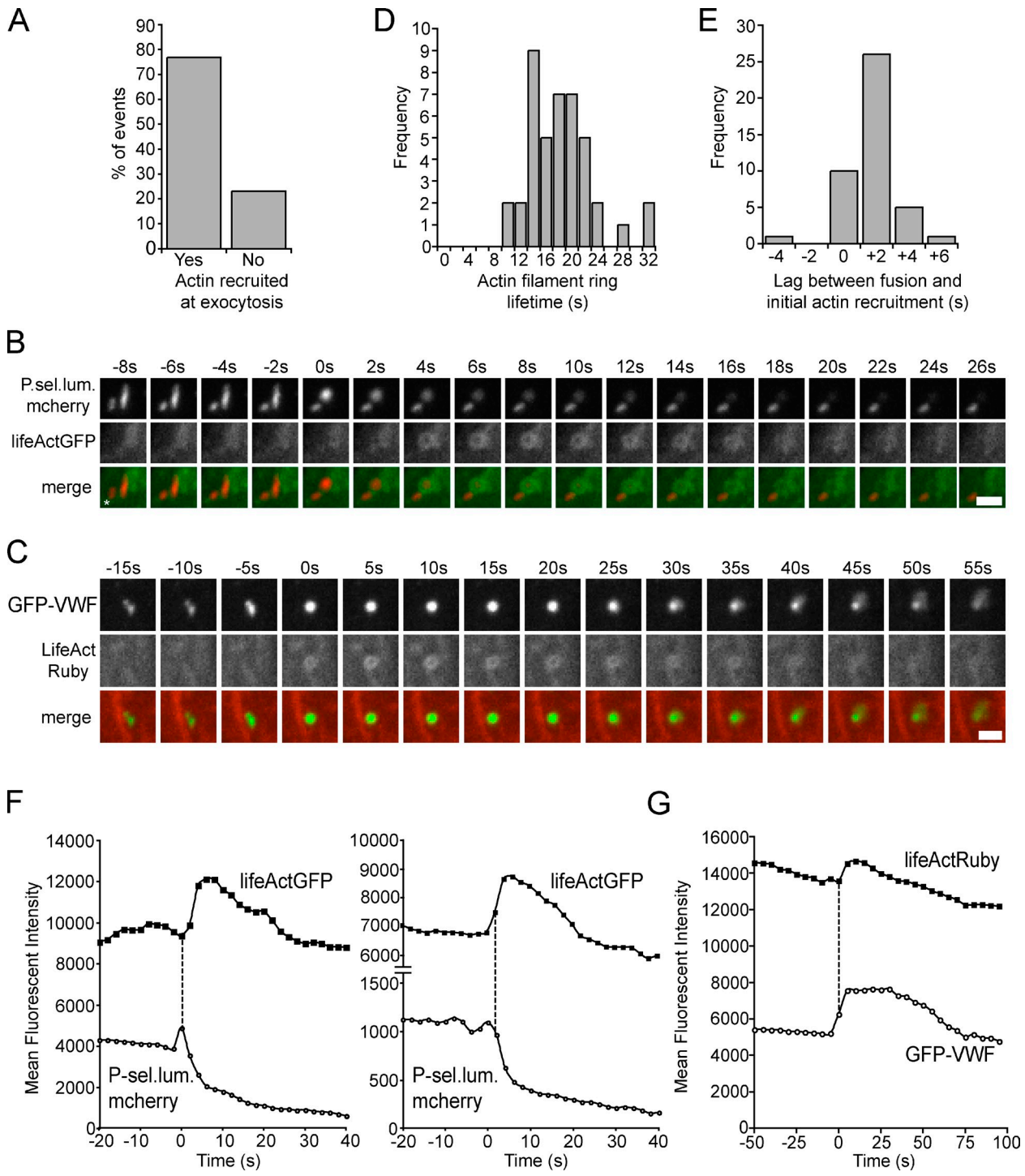

Figure 3. **Actin is recruited to WPBs during exocytosis.** (A–G) HUVECs coexpressing either Lifeact-GFP, a marker for actin filaments, and the mCherry–P-selectinLum (P.sel.lum.mcherry) domain (A, B, and D–F) or Lifeact-Ruby and GFP-VWF (C and G) stimulated with 100 ng/ml PMA and imaged live with a spinning-disk confocal microscope. Z stacks at a spacing of 0.5 µm were acquired every 2 s (A, B, and D–F) or 5 s (C and G) for 5 min, and images are all maximum intensity projections, except Lifeact channels in B and C, which are a single 0.5-µm-deep slices (see Materials and methods for a further explanation). Fusion is identified either by loss of mCherry fluorescence (A, D, and E) or by formation of rounded WPB structures (B, C, F, and G; assigned to 0 s in D–G). (A) Quantification of WPB fusion events in which Lifeact-GFP was recruited (plotted as the percentage of 143 total fusion events in nine cells). (B) Still images from a video that probes an individual WPB fusion event. The asterisk denotes a WPB that does not exocytose in the time course shown. (C) Still images from a video that probes an individual WPB fusion event and release of GFP-VWF contents. (D) Lifeact-GFP lifetime on individual WPBs (total of 43 WPBs in five cells). Actin filament ring total lifetime is defined as total time to reach peak fluorescence intensity and subsequent decay of signal. (E) Lag between WPB fusion and recruitment of Lifeact-GFP (total of 43 WPB fusion events in five cells). Initial actin recruitment is defined as the frame relative to fusion in which Lifeact fluorescence is first identified associated with the exocytosing WPB. (F) Change in mean fluorescence intensity of mCherry–P-selectinLum and Lifeact-GFP with the times of two WPB fusion events (the granule shown in B is plotted on the left trace). (G) For the WPB shown in C, change in mean fluorescence intensity with time of GFP-VWF and Lifeact-Ruby of the fusion and release of VWF content events. The dotted lines show the time points of WPB fusion. Bars, 2 µm.

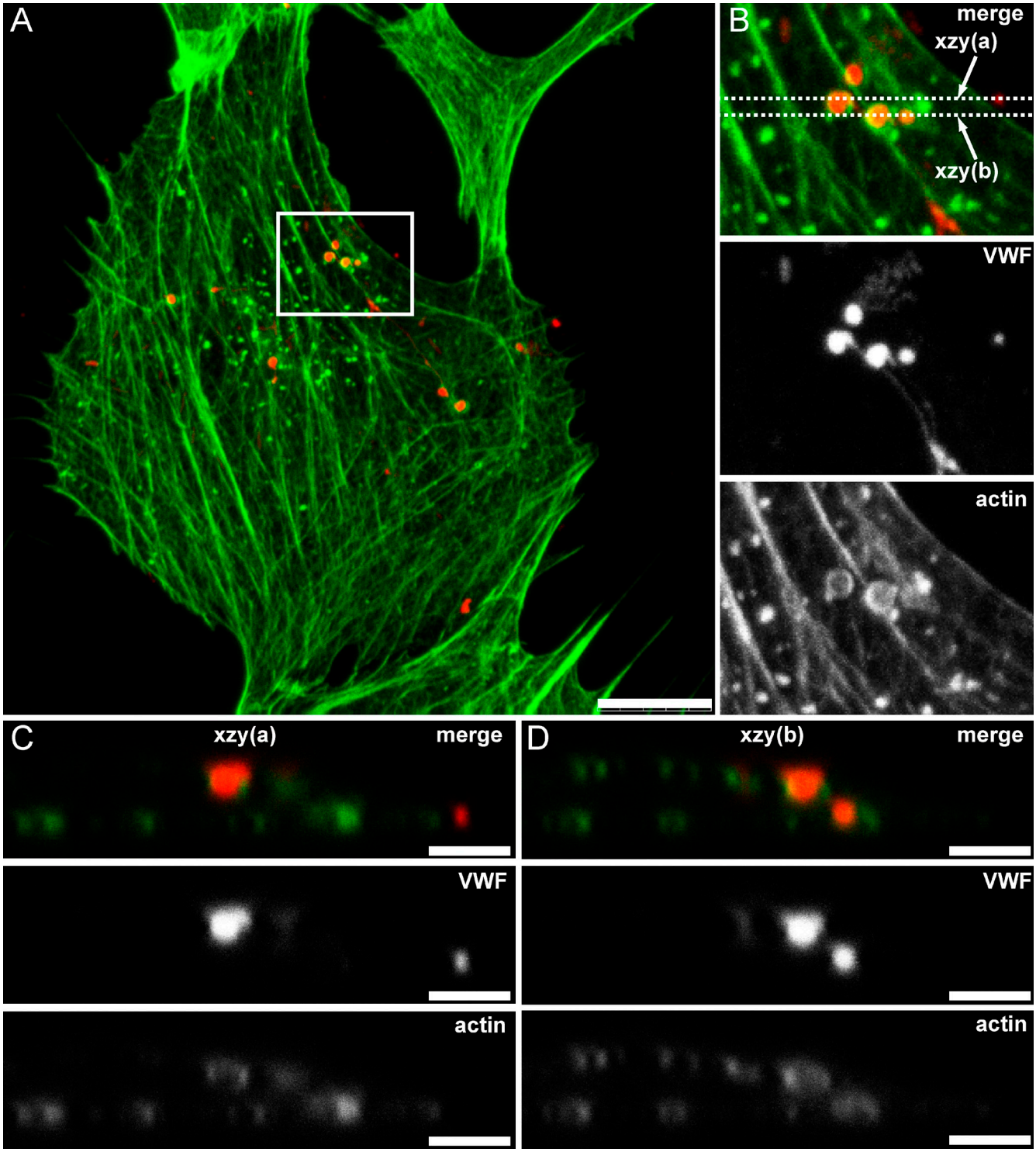

Figure 4. **Actin filaments are associated with one end of an individual WPB.** (A) Untransfected HUVECs were stimulated for 5 min with 100 ng/ml PMA and then fixed in formaldehyde with a procedure optimal for the actin cytoskeleton (see Materials and methods), costained for VWF (red) and phalloidin (green), and imaged on a confocal microscope. Images shown are maximum intensity projections. (B) Box region in A is shown at a higher magnification and illustrates WPB fusion events associated with actin filament rings. Dotted lines represent regions in which xzy sections were taken. (C and D) Xzy sections of the zoomed in region showing position of actin filaments relative to VWF. Bars: (A) 10 µm; (C and D) 2 µm.

of myosin II activity in addition to myosin light chain kinase are involved. Unfortunately, RNAi depletion of myosin II was not an effective method because depletion of myosin IIB induced a compensatory increase in myosin IIA, and we had little success in depleting all isoforms (unpublished data).

Secretory pores are open in cells treated with actin poisons

Is the loss of VWF release caused by a failure to exit through the secretory pore or because the secretory pore has closed as suggested by Bhat and Thorn (2009)? We used scanning and

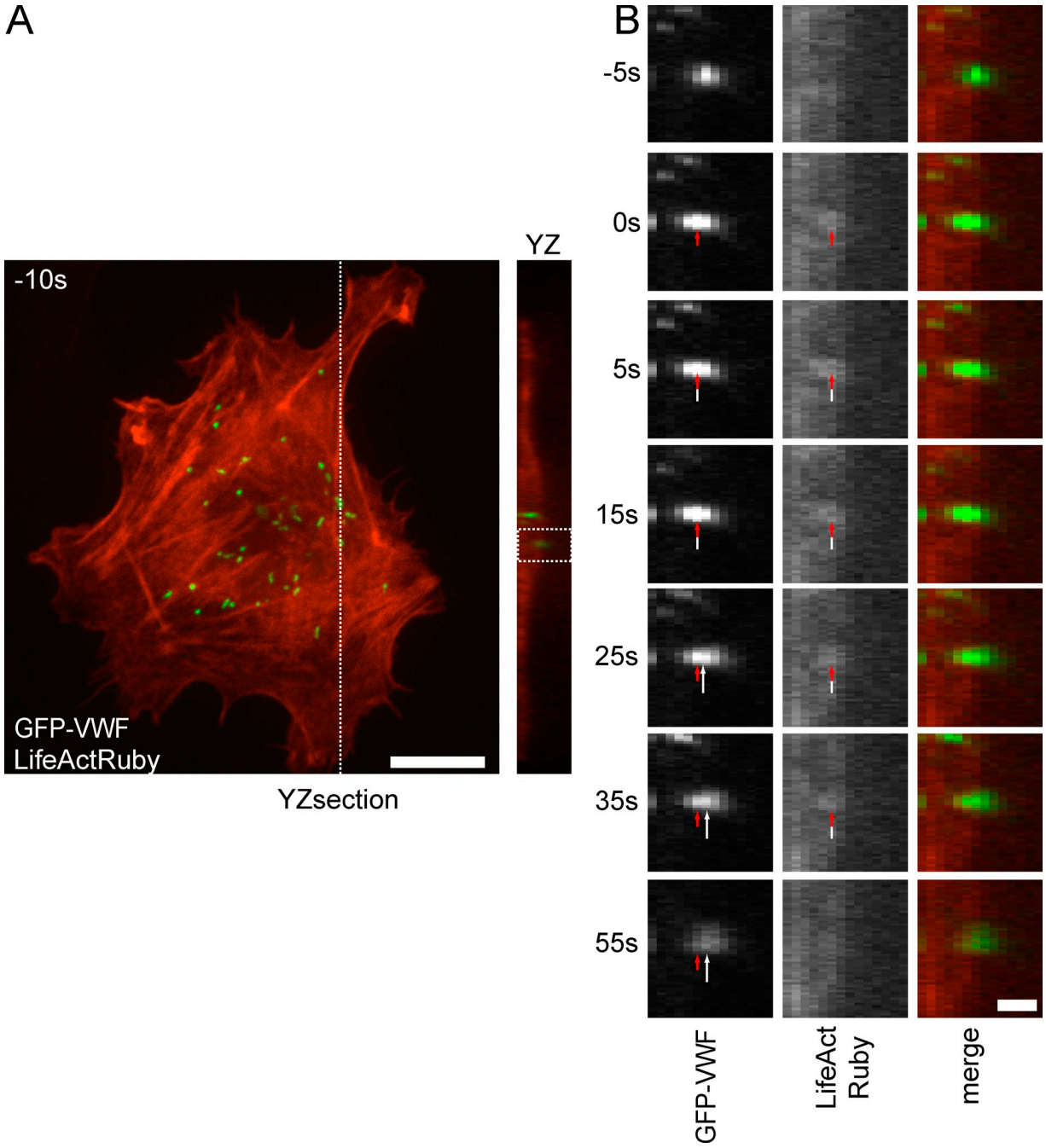

Figure 5. **Fused WPBs translocate out of the plane of the plasma membrane during WPB release of contents.** (A) Still from an xyz-projected view of WPB exocytosis. Inset shows the region in which the vertical (yz projection) was made in B. Time is relative to fusion (0 s). The dotted line shows the part of the cell in which a yz section was generated. The boxed region is shown at higher magnification and at a number of time points in B. Bar, 10 µm. (B) Time series of the organelle in the box in A as viewed in a vertical section. The short red arrows (0–55 s; GFP-VWF and Lifeact-Ruby time strips) indicate the position of the center of maximum fluorescence intensity within the WPBs or associated actin filaments at the point of fusion (0 s), and the long white arrows show the center at each new position (5–55 s). The WPB appears to translocate to the right. Actin filaments associated with WPBs appear to remain stationary with respect to the substratum. VWF and Lifeact-Ruby are single image planes. Bar, 1 µm.

transmission EM (TEM) to investigate the status of the VWF and pore in individual CCE-interrupted exocytic events. Scanning EM analysis of the surface of control secretagogue-stimulated HUVECs shows (Fig. 8 A) anti-VWF/colloidal gold–tagged strings of VWF (Fig. 8 A, i) emerging from structures comprised of membrane florets (Fig. 8 A, ii and iii), which is presumably a consequence of WPB fusion and/or the movement (Fig. 5) of fused WPBs (see Fig. S1 for images showing VWF gold staining separately). In CCE-treated cells (Fig. 8 B), the membrane florets and strings of the VWF protein are not detectable, but small clusters of gold-labeled VWF can be seen at the plasma membrane, consistent with its exposure via an open fusion pore (Fig. 8 B, i–iii).

We performed correlative light microscopy and EM with serial sectioning through exocytic structures in secretagogue-treated HUVECs (Fig. 8, C and D; and Fig. S2). In control cells

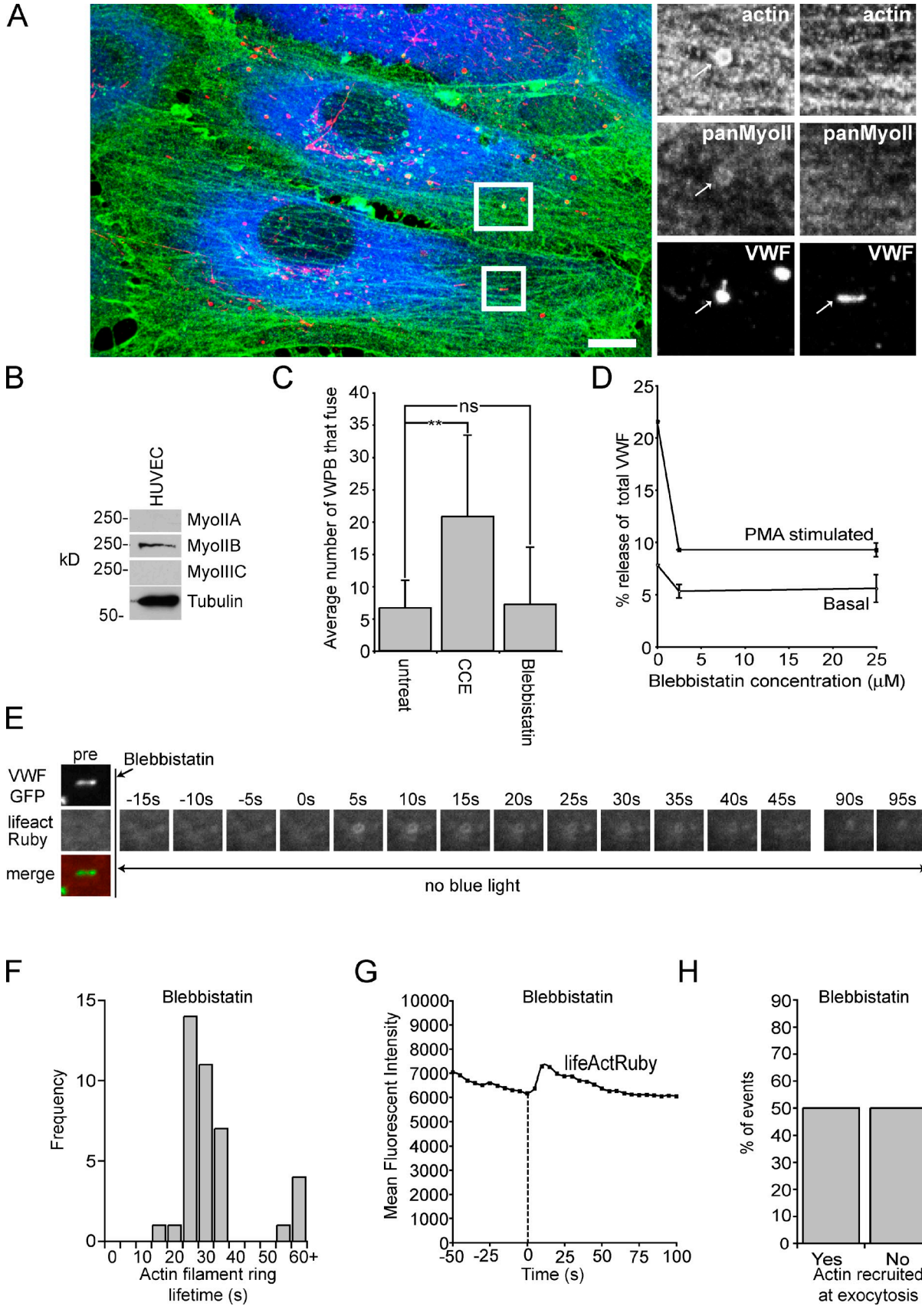

Figure 6. **Myosin II activity is required for the release of VWF contents.** (A) Untransfected HUVECs were stimulated for 5 min with 100 ng/ml PMA and then fixed in formaldehyde with a procedure optimal for imaging the actin cytoskeleton and myosin II (see Materials and methods), costained for pan–myosin II (panMyoII; blue), VWF (red), and actin (green), and imaged on a confocal microscope. The magnified insets on the right show an exocytosing WPB with

(Fig. 8 C), ∼500-nm-wide open pores are seen with VWF labeled with colloidal gold exiting. This exiting VWF extends from the pore to well above the plasma membrane (e.g., Fig. 8 C, v). In CCE-treated cells (Fig. 8 D), similar fusion pores are also clearly open. However, in contrast to controls, VWF fails to extend much beyond the open pore site (e.g., Fig. 8 D, v). This is even more apparent when the serial EM images are reconstructed into a single 3D image (Fig. 8, C and D, vi; and Videos 6 and 7). These data show that although the fusion pore is open (Fig. 8, A and C), VWF does not release (Fig. 2 and Fig. 8, B and D) in CCE-treated cells.

Discussion

In this paper, we assay both the fusion and content release stages of exocytosis alongside actin function, directly detecting and monitoring individual organelles by light microscopy and confirming key aspects by correlative EM. We have visualized single organelles at sufficient spatial and temporal resolution to monitor fusion of WPBs with the plasma membrane and subsequent release of VWF cargo independently.

Actin filaments initially prevent fusion of WPBs

We found that actin filaments initially act to inhibit secretion. The increase in the number of fused WPBs after drug-induced actin filament depolymerization (Fig. 2) is consistent with published data suggesting that WPBs are anchored via a ternary complex, including Rab27A/MyRIP (Nightingale et al., 2009), to the actin cytoskeleton to prevent premature fusion. A granule anchorage function for actin filaments has been proposed for several secretory cell types (Desnos et al., 2003; Waselle et al., 2003; Hume et al., 2007). The other inhibitory role postulated is that of a cortical actin barrier on exocytosis. We cannot completely rule out an inhibitory barrier function for cortical actin, but the close agreement between the extent of VWF release seen in Rab27a knockdown cells (Nightingale et al., 2009) and the increase in the number of fusion events documented here argues that, in endothelial cells at least, it plays a relatively minor role. Anchoring of granules to actin filaments may be particularly important in endothelial cells, in which there is a necessity for only mature granules to fuse, to maintain clinically essential levels of multimerization within VWF in plasma. A physical barrier would prevent exocytosis of both immature and mature granules equally, whereas anchoring to actin filaments might allow a degree of discriminatory regulation.

An actomyosin II filament ring associates with exocytosing WPBs to expel VWF cargo

After secretagogue stimulation, we demonstrated an additional actin-dependent function in supporting the release of the granule core protein VWF (Fig. 2 and Fig. 3). After WPB fusion with the plasma membrane, actin filaments are recruited to form a transient ring around/under the WPB (Fig. 3, Fig. 4, and Fig. 5). Actin filaments are also recruited to other fused organelles (Valentijn et al., 2000b; Sokac et al., 2003; Miklavc et al., 2009). In all these situations, the actin serves to coat the organelle rather than forming the ring-like structure we noted at WPB exocytosis (Fig. 4).

Several functions have been proposed for actin filaments recruited to exocytic organelles after fusion in other cells (see Introduction for details; Segawa and Yamashina, 1989; Valentijn et al., 2000b; Sokac et al., 2003; Nemoto et al., 2004; Schietroma et al., 2007; Bhat and Thorn, 2009). However, in these studies, endogenous cargo release was not probed, or cargo and actin were not visualized directly together with an appropriate temporal resolution to allow identification of exactly when actin could act with respect to cargo release. Our new data directly correlate with high precision the release of endogenous cargo with the time at which actin functions.

These data lead us to a model in which an actin filament ring acts as a minicytokinetic ring to exert force on the bottom of an open granule, helping to push VWF out of the other end into the extracellular environment. First, the appearance, duration, and disappearance of the actin filament ring approximately mirrors the initiation and continued release of VWF cargo (Fig. 3 and Fig. 5). Second, we have localized myosin II at the actin ring during exocytosis (Fig. 6 A). Third, we know from our temporal analysis of fusion and content release in live HUVECs that myosin II ATPase is required at the same step as the actin ring to release VWF cargo from organelles after they have fused (Fig. 6 and Fig. 7). Critically, actin ring dynamic behavior is also tightly linked to the ∼600-nm movement of fused WPBs relative to the plasma membrane, which in turn, correlates with VWF release from that same WPB (Fig. 5). Furthermore, to extrude content in this way requires that actin filament ring

an actin ring and a WPB in a similar part of the cell yet to exocytose with no actin ring. Images shown are maximum intensity projections. The arrows highlight the recruitment of actin and myosin to the exocytosing VWF in the first three images. But in a situation in which VWF is not released (the next three images), actin and myosin are not recruited. Bar, 10 µm. (B) Western blot analysis of myosin II isotypes in HUVECs. (C) HUVECs expressing the mCherry–P-selectinLum domain were stimulated with 100 ng/ml PMA for 10 min with or without a 5-min preincubation with 25 µM blebbistatin. Mean number of individual WPB fusion events in 300 s (control: $n = 11$ cells; blebbistatin: $n = 6$ cells; **, $P = 0.004$; ns, $P = 0.863$; t test). Error bars show SDs. (D) Quantification of VWF secretion at different blebbistatin concentrations. Error bars represent SDs. (E–H) HUVECs coexpressing VWF-GFP and Lifeact-Ruby were imaged before treatment with blebbistatin, preincubated with 25 µM blebbistatin for 2 min, and then stimulated with 100 ng/ml PMA for 10 min (in the continued presence of blebbistatin). During blebbistatin treatment, time-lapse images were only acquired from the Lifeact-Ruby (i.e., no blue light was present). A final image was then acquired from both markers. (E) Still images from a video of individual WPB fusion and blebbistatin-inhibited release of VWF in live cells. Bar, 2 µm. (F) Actin filament ring total lifetime, defined as total time to reach peak fluorescence intensity and subsequent decay of signal, in blebbistatin-treated cells (plotted from 39 actin-positive fusion events in six cells). (G) Quantification of intensity of fluorescence of Lifeact-Ruby for the individual organelle shown in E. The dotted line shows the time point of WPB fusion. (H) Quantification of WPB fusion events in which Lifeact-Ruby was recruited (plotted as the percentage of 82 total fusion events in six cells) to WPBs in the presence of blebbistatin. Note that blocking myosin II has no effect on the fusion of WPBs yet blocks subsequent secretion of VWF from the same fused organelle and extends the lifetime of the actin filament ring. In all parts of this figure, blebbistatin treatment of cells was performed in the absence of any blue light, except for the final image in E (labeled post).

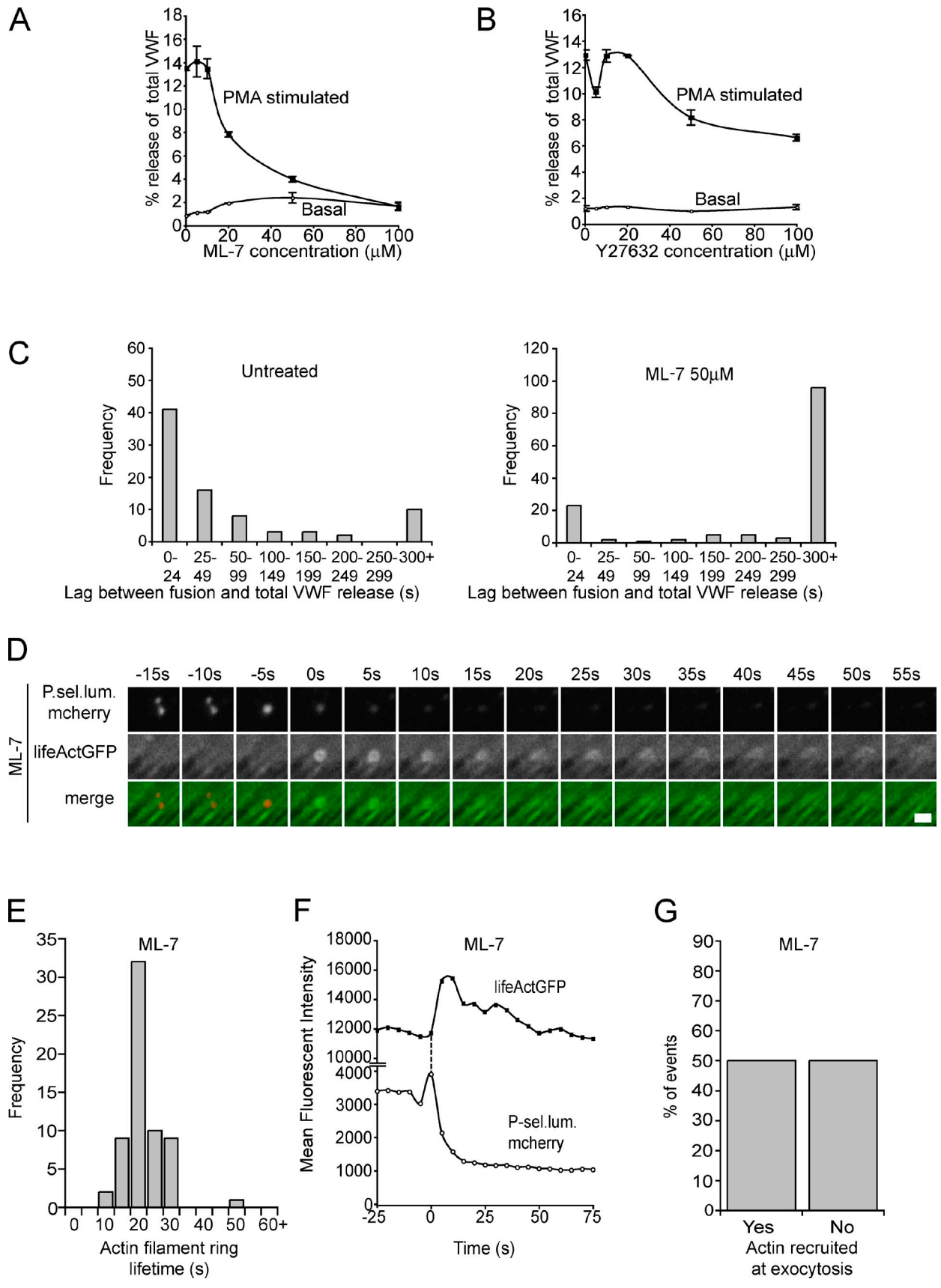

Figure 7. **Myosin light chain kinase activity is required for the release of VWF contents.** (A–G) HUVECs coexpressing GFP-VWF and the mCherry–P-selectinLum domain were stimulated with 100 ng/ml PMA for 10 min with or without a 15-min preincubation with 50 µM ML-7 (A and C–G) or treated with Y27632 (B). Fusion is assigned to 0 s. (A) Quantification of VWF secretion at different ML-7 concentrations. (B) Quantification of VWF secretion at

position is polarized toward the distal end of the granule as observed (Fig. 5 and Fig. 6). This model is also consistent with the failure of VWF to move out of open pores (Fig. 8 B) or to form strings (Fig. 2) when cells are treated with an inhibitor of actin assembly. Mathematical modeling also suggests that contractile force can be driven via polymer disassembly (Mogilner and Oster, 2003), which is not inconsistent with some of our data (Fig. 2 and Fig. 3) and may contribute to actomyosin II–based force. The actin-dependent movement of VWF out of fused granules may also underlie the notable membrane florets that form at the exocytic site (Fig. 8 A), as such structures are absent in the scanning EM of CCE-treated cells. In vivo, the intravascular blood flow would also help to unfurl VWF into platelet-catching strings connected to the surface of endothelial cells.

Other potential roles for myosin II for exocytosing granules

In other situations, actomyosin II contractility is instead thought to hold open the pore at exocytosis (Larina et al., 2007; Bhat and Thorn, 2009). We have little evidence for this function in VWF secretion: analysis of pore structure after exocytosis in the presence of an actin-depolymerizing agent shows multiple arrested open pores, and more pores are noted than in untreated cells (Fig. 2 E and Fig. 8). The pore size appears similar in gross size to those of untreated cells (~500 nm), but we did note pieces of membrane that partially obscured parts of the pore. We regard these as pieces of membrane that would ordinarily be pushed from the mouth of the pore at exocytosis. Given the observed large size of the WPB fusion pore, we cannot view these flaps as likely to impede release of VWF. Furthermore, the observed position of the actin filament ring toward the base of the WPB (Fig. 4) means, conceptually, it is less likely to stabilize the fusion pore/keep the pore open, as it is not directly present at the plasma membrane.

In *Xenopus laevis* oocytes, actomyosin II associated with fused granules is thought to drive a later process—compression of granule membrane during compensatory endocytosis that occurs after cargo has been released. We do not have a direct measure of the timing of any reendocytosis of WPBs in endothelial cells and cannot rule out such a possibility. However, F-actin rings around exocytosing WPBs disappear around the time that the last of the VWF is released, implying that the ring in endothelial cells may not persist long enough to also be involved in reendocytosis in these cells.

Mechanism of assembly and turnover of the F-actin ring associated with WPBs

We did not detect any actin filament translocation toward the WPB membrane, suggesting that actin filaments are directly nucleated and assembled on the surface of the organelle. In PC12 cells, Arp2/3 is localized to secretory granules and likely nucleates actin filaments on these granules in these cells (Gasman et al., 2004), and in cortical granules, neural Wiskott-Aldrich Syndrome protein and cdc42 have shown to be necessary for coat formation (Sokac et al., 2003). However, knockdown of Arp3 has no effect on regulated release of VWF, and Arp3 is not localized to WPBs (unpublished data). Thus, actin filament formation on granules may be regulated differently in different cells.

The WPB actin ring is exceptionally dynamic, completely forming and disassembling within a mean of ~20 s. Actin filament coats on other regulated secretory organelles vary in stability, with actin recruitment in cortical granules appearing similarly dynamic (Sokac et al., 2003) but actin recruitment on lamellar bodies appearing markedly slower (Miklavc et al., 2009). Outside of secretory organelles, highly dynamic actin filaments, e.g., within leading edge protrusions in motile cells, turn over with a half-life of 1–3 min, much slower than the WPB actin ring. Inhibition of actin filament disassembly (Fig. 2) or myosin II activity (Fig. 6) both significantly extend the duration of the WPB actin filament ring. Thus, although the myosin II force is not required to form the actin ring, actomyosin II contractility may augment actin filament ring depolymerization. Certainly, myosin II–dependent actin filament turnover occurs within dividing (Guha et al., 2005; Murthy and Wadsworth, 2005) and in motile cells (Vallotton et al., 2004; Medeiros et al., 2006; Wilson et al., 2010).

The extent to which actin filament force-based extrusion of cargo is a general mode of action for cells other than HUVECs remains to be directly determined. That actin filaments have been identified on both small and large granules in several cell types is perhaps indicative of wide-ranging importance. In the endothelial cell, a large amount of protein content must be secreted into the lumen of the blood vessel to quickly recruit platelets. It is also possible that, for this reason, a special mode of secretion had to be adopted, and perhaps, secretion of surfactant from lung cells (Miklavc et al., 2009) with its unique hydrophobic properties may present a similar burden on the exocytic machinery. We would argue that only by distinguishing and imaging exocytosis at both fusion and release of cargo steps directly alongside the analysis of actin dynamics during exocytosis can prefusion actin-dependent anchoring be separated from the postfusion augmentation of content release.

Materials and methods

Cell culture and nucleofection

HUVECs were cultured as described previously (Michaux et al., 2006a). GFP-VWF (Romani de Wit et al., 2003) was a gift from J. Voorberg and J.A. Van Mourik (Sanquin Research Laboratory, Amsterdam, Netherlands).

different Y27632 concentrations. (C) Lag between WPB fusion and full release of GFP-VWF for individual WPBs in live PMA-stimulated cells in the presence (137 fusion events in nine cells) or absence (83 fusion events in 11 cells) of ML-7. 300+ s indicates that VWF failed to release during 600 s of time-lapse filming. (D) Still images from a video of an individual WPB fusion event in ML-7–inhibited cells cotransfected with mCherry–P-selectinLum (P.sel.lum.mcherry) and Lifeact-GFP. Bar, 2 µm. (E) Actin filament ring total lifetime, defined as total time to reach peak fluorescence intensity and subsequent decay of signal, in ML-7–treated cells (plotted from 63 actin positive fusion events from six cells). (F) Quantification of intensity of fluorescence of mCherry–P-selectinLum and Lifeact-GFP for the individual organelle shown in D. The dotted line shows the time point of WPB fusion. (G) Quantification of WPB fusion events in which Lifeact-GFP was recruited (plotted as the percentage of 142 total fusion events in six cells) to WPBs in the presence of ML-7. Error bars represent SDs.

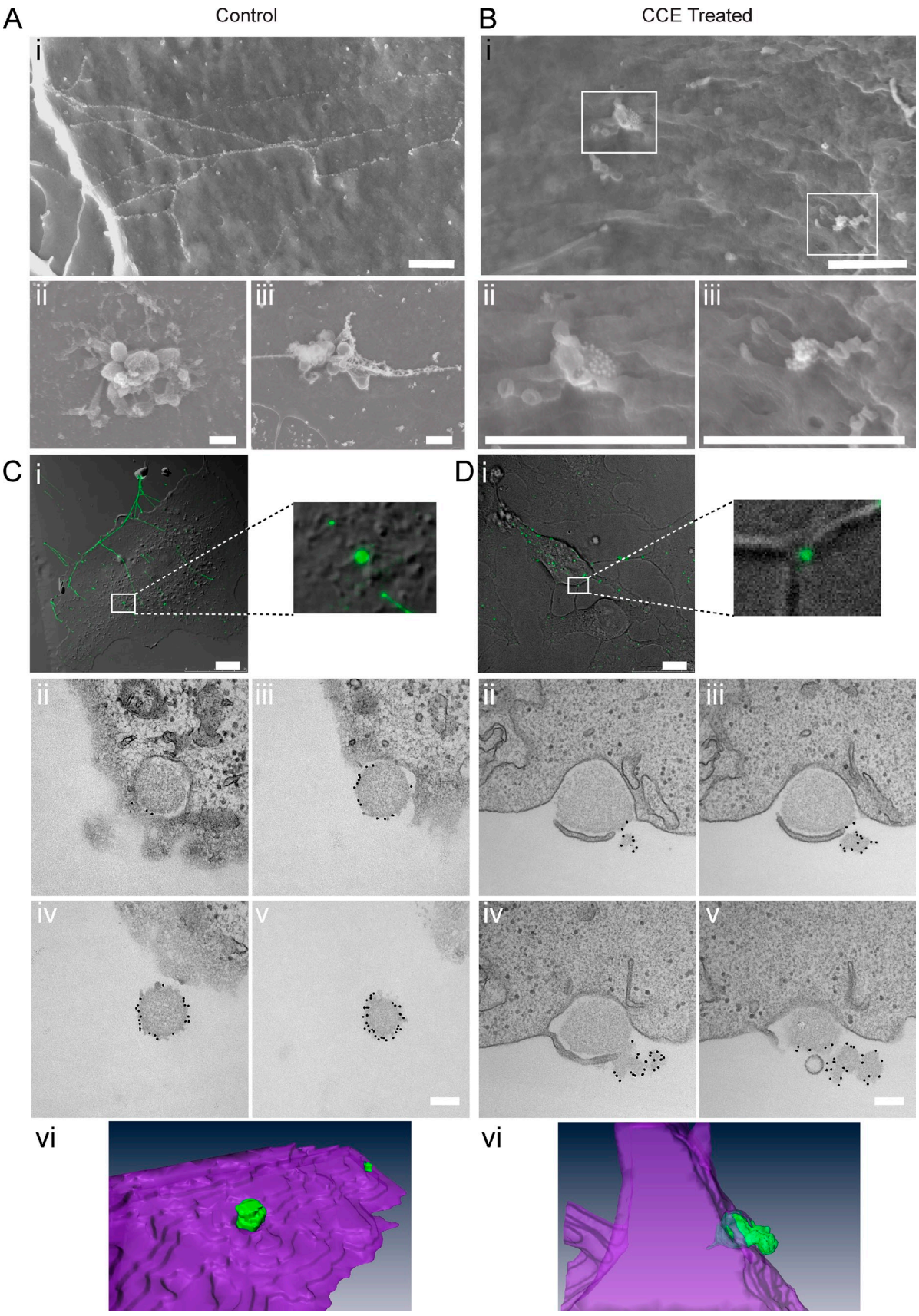

Figure 8. **Ultrastructural analysis of WPBs during exocytosis.** (A–D) HUVECs were stimulated with 100 ng/ml PMA for 10 min (A and C) or pretreated with 1 µM CCE for 15 min before PMA stimulation (B and D) and then labeled for released VWF (15-nm gold [A and B] or 15-nm gold and Alexa Fluor 488 nm [C and D]). (A) Scanning EM of PMA-stimulated HUVECs shows a network of VWF strings (i) and marked membrane ruffling (ii and iii) that appear

The C terminal–tagged P-selectinLum–mCherry fusion construct was generated by amplification from a P-selectin luminal PRK5 construct (Harrison-Lavoie et al., 2006) using primers encoding flanking 5′ BglII and 3′ SmaI sites. The product was digested with BglII and SmaI and ligated into pmCherry N1 vector (Takara Bio Inc.) digested with BglII and EcoRV. Lifeact-GFP (Riedl et al., 2008) and Lifeact-Ruby were gifts from B. Baum (University College London, London, England, UK). DNA (typically 1–5 µg) was transfected into HUVECs by nucleofection using the program U-001 (Lonza). Cells were typically assayed 24 h after transfection.

Antibodies for immunofluorescence

Rabbit anti-VWF (1 in 10,000) was purchased from Dako. Sheep anti-VWF (1 in 10,000) was purchased from AbD Serotec. Rabbit anti–myosin IIA, –myosin IIB, and –myosin IIC (1 in 200) were purchased from Cell Signaling Technology. Rabbit pan–myosin II (1 in 50) was obtained from Biogenesis. Mouse antiactin (clone C4; 1 in 200) was purchased from MP Biomedicals. Alexa Fluor 488- and 568-nm fluorescent conjugates (1 in 500) and Alexa Fluor 488-nm conjugated phalloidin were obtained from Invitrogen. Cy5 fluorescent conjugates (1 in 200) were purchased from Jackson ImmunoResearch Laboratories, Inc.

Immunofluorescence

For standard fixation, cells were fixed at 37°C in 4% methanol-free formaldehyde (TAAB Laboratories Equipment, Ltd.) in cytoskeleton buffer (10 mM MES, pH 6.1, 3 mM $MgCl_2$, 138 mM KCl, and 2 mM EGTA) with 0.32 M sucrose and then permeabilized in 0.5% Triton X-100 and incubated with Alexa Fluor 488–conjugated phalloidin (Invitrogen) and a relevant primary antibody. For myosin II staining, cells were fixed in cytoskeleton buffer with 0.32 M sucrose and 4% methanol-free formaldehyde supplemented with 0.1% Triton X-100 and 2 µg/ml phalloidin. Cells were then postfixed in methanol at −20°C for 3 min and incubated with the relevant primary antibodies. The cells were then rinsed, and a 488-nm, 568-nm, or Cy5 secondary antibody was added before mounting with antifade reagent containing DAPI (ProLong; Invitrogen). This method optimally preserves the cytoskeleton (Cramer and Mitchison, 1993). Mounted coverslips were imaged at an ambient temperature through a 63× oil immersion lens (NA 1.3) on a confocal system (TCS SPE; Leica).

Western blotting

Proteins were separated by SDS-PAGE, transferred to Whatman nitrocellulose membranes (PerkinElmer), and then probed with the following antibodies: rabbit anti–myosin IIA, –myosin IIB, and –myosin IIC (1 in 1,000); mouse antitubulin antibodies (1 in 500) purchased from Sigma-Aldrich; and rabbit anti-VWF (1 in 500). Then, nitrocellulose membranes were incubated with the appropriate anti–rabbit or –mouse HRP-conjugated secondary antibodies (1 in 5,000) purchased from Jackson ImmunoResearch Laboratories, Inc.

Secretion assay and ELISA

HUVECs were incubated with 1 µM CCE, 0–25 µM blebbistatin, 0–100 µM Y27632, or 0–100 µM ML-7 (Sigma-Aldrich) for 5–15 min before determining VWF release. The VWF secretion assay has been described previously (Lui-Roberts et al., 2005). In short, cells were rinsed and incubated in serum-free medium in the presence or absence of 100 ng/ml PMA (Sigma-Aldrich) and/or the relevant drug for 30 min. The medium was collected, and the remaining cells were then lysed to determine total VWF levels. Relative amounts of VWF were determined by ELISA (Blagoveshchenskaya et al., 2002). MaxiSorp plates (Thermo Fisher Scientific) were coated with the rabbit anti-VWF antibody (Dako) and blocked before addition of the basal, stimulated, and lysate samples alongside serially diluted human plasma as a VWF standard. Plates were washed, and a rabbit anti-VWF antibody conjugated to HRP was added (Dako). After further rounds of washing, the plate was developed with *o*-phenylenediamine dihydrochloride and hydrogen peroxide in a citrate phosphate buffer. Absorbance was analyzed at 450 nm in a thermomax microplate reader (Molecular Devices) using a kinetic protocol with a reading every 30 s for 30 min. Basal and stimulated releases were presented as a percentage of total VWF present in the cells (basal releasate + stimulated releasate + remainder present in the lysate).

Live-cell imaging

Nucleofected cells were plated in 4-well coverglass chamber slides (Thermo Fisher Scientific) and imaged in a heat-controlled chamber at 37°C in HUVEC growth media. The cells were pretreated with or without the relevant drugs, 25 µM blebbistatin (2 min), 1 µM CCE (15 min), or 50 µM ML-7 (15 min), before stimulating with 100 ng/ml PMA (while maintaining the appropriate drug concentration). Cells were visualized using a 100× oil immersion lens (NA 1.4) on an spinning-disk system (UltraVIEW VoX; PerkinElmer) mounted on an inverted microscope (TiE; Nikon) with an EM charge-coupled device camera (512 × 512 pixels; C9100-13; Hamamatsu Photonics) and 488- and 561-nm solid-state lasers. Z stacks were acquired using a piezo (NanoScanZ; Prior Scientific) every 2–5 s for 5–10-min periods with a step size of 0.4–0.5 µm, comprising 9–14 pictures (depending on cell height) with an exposure for each image at 30 ms. Images were analyzed, and maximum intensity and yz projections were generated in Volocity (version 5.3.1; PerkinElmer). In Fig. 3 and Fig. 6, single image planes from a z stack are shown to illustrate the actin filament ring that forms at the bottom of WPBs, whereas maximum intensity projections of the entire stack are used to illustrate the WPB. This is the optimal way of displaying all of the information during exocytosis; WPBs are larger (1–5 µm) than a single image plane (0.5 µm) and, thus, capturing the entire WPB structure requires several planes. In addition, this will also capture VWF, as it starts to diffuse away from fused WPBs. Actin filament rings associated with WPBs are only 0.5–1 µm and, thus, are captured in only 1–2 image planes. In addition, there is an abundance of other actin filament structures in other image planes that are not associated with fused WPBs, e.g., stress fibers and any maximum intensity projection would portray these irrelevant actin filament structures from other spatial locations.

Quantification of exocytosis videos

Loss of mCherry–P-selectinLum was used mainly as a marker of fusion, as this reports only the fusion step. However, to compare GFP-VWF release of contents with actin filament behavior (Fig. 3, Fig. 4, Fig. 5, and Fig. 6), we instead chose rounded WPB shape or transient increase in GFP-VWF as markers of fusion. The lag between fusion and total VWF release was defined as the time between loss of P-selectinLum–mCherry to the loss of GFP-VWF fluorescence at the exocytic site. Data are displayed as a frequency distribution of all exocytic events from several cells, and therefore, error bars are not appropriate.

Volocity (version 5.3.1) was used to determine mean fluorescence intensity of the transfected proteins during exocytosis. In both analysis protocols, quantification was performed on maximum intensity projections. In situations in which we needed to determine the integrated mean fluorescent intensity of two WPB-specific fluorescent probes during the process of exocytosis (Fig. 1), we defined the relevant region by intensity (1.478 for the 488-nm line and 0.919 for the 561-nm line). We then used a fine median filter to remove the background and excluded any regions <0.05 μm^3. The mean fluorescent intensity was then determined for the defined region. A same-size region outside the cell was used to determine a background fluorescence at each of the time points and was subtracted to give the final intensity values.

When imaging the exocytosis of a fluorescent protein in relation to actin (Fig. 3 and Fig. 6), we determined the mean fluorescence intensity across a region of interest defined as the minimal region that comprised both the WPB and actin ring fluorescence. A same-size region outside the cell was used to determine a background fluorescence at each of the time points, and this was subtracted to give the final intensity values. Mean fluorescence

to be sites of WPB exocytosis and initial VWF string release. These strings and sites are extensively labeled with anti-VWF/gold (see Fig. S1 for backscatter images showing VWF gold labeling). (B, i) CCE-treated cells show a marked absence of VWF strings. Instead, only small patches of intense gold labeling are present with no membrane ruffling, indicating the WPBs have fused but failed to release VWF as strings. (ii and iii) Magnified regions of the areas described by the white boxes. (C and D, i) Differential interference contrast images overlayed with a fluorescent image of VWF labeling (green). A specific exocytic site is magnified in the white boxed region. (C and D, ii–v) Serial TEM sections of the exocytic site shown in C and D (i) with v being the highest section. (C and D, vi) 3D reconstruction of the serial sections shown above. The reconstructions are also shown as Videos 6 and 7, revealing the same exocytic structures from a variety of angles. For the reconstruction, the VWF is highlighted in green, whereas the remainder of the cell is purple. Note that the VWF is released normally in the untreated cell, whereas the VWF in the drug-treated cell appears to be incompletely exocytosed. Fluorescent images are maximum intensity projections. All the serial TEM sections are shown in Fig. S2. Bars: (A and B, i–iii) 1 µm; (C and D, i) 10 µm; (C and D, ii–v) 200 nm.

values obtained therefore represent the mean fluorescence across the whole region of interest. WPB-specific probes will therefore have a lower fluorescence intensity than for the protocol used in Fig. 1.

Correlative light and TEM

HUVECs were plated into gridded coverslip–bottomed dishes (MatTek) and, 24 h later, pretreated for 15 min with or without 1 µM CCE followed by stimulation with 100 ng/ml PMA for 10 min. Cells were fixed and stained with rabbit anti-VWF followed by labeling with both an Alexa Fluor 488-nm secondary antibody and protein A–gold (15 nm). Cells were then imaged in 0.1 M cacodylate using a 20× air (NA 0.7), 40× oil (NA 1.25), and 63× oil (NA 1.4) immersion objectives on a confocal microscope (SP5; Leica) at an ambient temperature. Fluorescent z stacks and differential interference contrast images were acquired to identify the same cell by TEM. The coverslips were fixed in EM-grade 2% paraformaldehyde, 2% glutaraldehyde (TAAB Laboratories Equipment, Ltd.) secondarily fixed in 1% osmium tetraoxide, and 1.5% potassium ferricyanide and then tannic acid treated. Samples were then dehydrated and embedded in Epon resin. Coverslips were inverted onto prepolymerized Epon stubs and polymerized by baking at 60°C overnight. The cells of interest were found on the block surface by using the grid marks transferred from the coverslip, and the light microscopy images and serial 70-nm-thin sections were cut with a diatome 45° diamond knife using an ultramicrotome (UC7; Leica). Ribbons of sections were collected on 1 × 2–mm Formvar-coated slot grids and stained with Reynolds lead citrate. Samples were imaged using a transmission electron microscope (Tecnai G2 Spirit; FEI) and a charge-coupled device camera (SIS Morada; Olympus). The serial sections were aligned and reconstructed into a 3D projection using Amira 5.2.2 software (Visage).

Scanning EM

HUVECs were grown on glass coverslips and treated as for TEM until dehydration. The samples were then critically point dried using a point drying apparatus (Polaron E3100; Quorum Technologies, Ltd.) mounted onto 12.5-mm-diam aluminum stubs using electrodag (silver DAG; Agar Scientific) and coated with a 2–3-nm-thick layer of carbon using an ion beam coater (Gatan, Inc.). Samples were examined at 5.0 kV on a high-resolution field emission-scanning electron microscope (JSM-7401F; JEOL).

Online supplemental material

Fig. S1 shows scanning EM secondary electron images of VWF strings at exocytosis alongside backscattered electron images that show VWF gold labeling. Fig. S2 shows all serial TEM sections used for the 3D reconstructions shown in Fig. 8 (C and D, vi). Fig. S3 shows the effect of blebbistatin treatment on actin ring recruitment, lifetime, and VWF exocytosis while imaging with blue light. Video 1 shows an unstimulated HUVEC transfected with GFP-VWF and mCherry–P-selectinLum domain as visualized by spinning-disk confocal microscopy over a 10-min period. Video 2 shows a PMA-stimulated HUVEC transfected with GFP-VWF and mCherry–P-selectinLum domain as visualized by spinning-disk confocal microscopy over a 10-min period. Video 3 shows a HUVEC transfected with GFP-VWF and mCherry–P-selectinLum domain after pretreatment with CCE and stimulation with PMA as visualized by spinning-disk confocal microscopy over a 10-min period. Video 4 shows a HUVEC transfected with Lifeact-GFP and mCherry–P-selectinLum domain after stimulation with PMA as visualized by spinning-disk confocal microscopy over a 5-min period. Video 5 shows a yz slice of a HUVEC transfected with Lifeact-Ruby and GFP-VWF exocytosing after stimulation with PMA as visualized by spinning-disk confocal microscopy. Video 6 shows an animation of the 3D reconstruction shown in Fig. 8 C (vi). Video 7 shows an animation of the 3D reconstruction shown in Fig. 8 D (vi). Online supplemental material is available at http://www.jcb.org/cgi/content/full/jcb.201011119/DC1.

The authors would like to thank Marie O'Connor for helping with graphing and statistics and Jemima Burden, Lauren McLaughlin, and Andrew Vaughan for technical assistance.

T.D. Nightingale, I.J. White, E.L. Doyle, K.J. Harrison-Lavoie, K.F. Webb, and D.F. Cutler were supported by the Medical Research Council of Great Britain (grant U12260000200001 to D.F. Cutler). L.P. Cramer was supported by Cancer Research UK (grant code C8691) and a Royal Society University Research Fellowship.

Submitted: 23 November 2010
Accepted: 18 July 2011

References

Andzelm, M.M., X. Chen, K. Krzewski, J.S. Orange, and J.L. Strominger. 2007. Myosin IIA is required for cytolytic granule exocytosis in human NK cells. *J. Exp. Med.* 204:2285–2291. doi:10.1084/jem.20071143

Babich, V., A. Meli, L. Knipe, J.E. Dempster, P. Skehel, M.J. Hannah, and T. Carter. 2008. Selective release of molecules from Weibel-Palade bodies during a lingering kiss. *Blood.* 111:5282–5290. doi:10.1182/blood-2007-09-113746

Berberian, K., A.J. Torres, Q. Fang, K. Kisler, and M. Lindau. 2009. F-actin and myosin II accelerate catecholamine release from chromaffin granules. *J. Neurosci.* 29:863–870. doi:10.1523/JNEUROSCI.2818-08.2009

Bhat, P., and P. Thorn. 2009. Myosin 2 maintains an open exocytic fusion pore in secretory epithelial cells. *Mol. Biol. Cell.* 20:1795–1803. doi:10.1091/mbc.E08-10-1048

Bittins, C.M., T.W. Eichler, and H.H. Gerdes. 2009. Expression of the dominant-negative tail of myosin Va enhances exocytosis of large dense core vesicles in neurons. *Cell. Mol. Neurobiol.* 29:597–608. doi:10.1007/s10571-009-9352-z

Blagoveshchenskaya, A.D., M.J. Hannah, S. Allen, and D.F. Cutler. 2002. Selective and signal-dependent recruitment of membrane proteins to secretory granules formed by heterologously expressed von Willebrand factor. *Mol. Biol. Cell.* 13:1582–1593. doi:10.1091/mbc.01-09-0462

Bonfanti, R., B.C. Furie, B. Furie, and D.D. Wagner. 1989. PADGEM (GMP140) is a component of Weibel-Palade bodies of human endothelial cells. *Blood.* 73:1109–1112.

Burgoyne, R.D., and A. Morgan. 2003. Secretory granule exocytosis. *Physiol. Rev.* 83:581–632.

Charras, G.T., C.K. Hu, M. Coughlin, and T.J. Mitchison. 2006. Reassembly of contractile actin cortex in cell blebs. *J. Cell Biol.* 175:477–490. doi:10.1083/jcb.200602085

Cingolani, L.A., and Y. Goda. 2008. Actin in action: the interplay between the actin cytoskeleton and synaptic efficacy. *Nat. Rev. Neurosci.* 9:344–356. doi:10.1038/nrn2373

Cramer, L.P. 1999a. Organization and polarity of actin filament networks in cells: implications for the mechanism of myosin-based cell motility. *Biochem. Soc. Symp.* 65:173–205.

Cramer, L.P. 1999b. Role of actin-filament disassembly in lamellipodium protrusion in motile cells revealed using the drug jasplakinolide. *Curr. Biol.* 9:1095–1105. doi:10.1016/S0960-9822(99)80478-3

Cramer, L., and T.J. Mitchison. 1993. Moving and stationary actin filaments are involved in spreading of postmitotic PtK2 cells. *J. Cell Biol.* 122:833–843. doi:10.1083/jcb.122.4.833

Deng, Z., T. Zink, H.Y. Chen, D. Walters, F.T. Liu, and G.Y. Liu. 2009. Impact of actin rearrangement and degranulation on the membrane structure of primary mast cells: a combined atomic force and laser scanning confocal microscopy investigation. *Biophys. J.* 96:1629–1639. doi:10.1016/j.bpj.2008.11.015

Desnos, C., J.S. Schonn, S. Huet, V.S. Tran, A. El-Amraoui, G. Raposo, I. Fanget, C. Chapuis, G. Ménasché, G. de Saint Basile, et al. 2003. Rab27A and its effector MyRIP link secretory granules to F-actin and control their motion towards release sites. *J. Cell Biol.* 163:559–570. doi:10.1083/jcb.200302157

Dong, J.F., J.L. Moake, L. Nolasco, A. Bernardo, W. Arceneaux, C.N. Shrimpton, A.J. Schade, L.V. McIntire, K. Fujikawa, and J.A. López. 2002. ADAMTS-13 rapidly cleaves newly secreted ultralarge von Willebrand factor multimers on the endothelial surface under flowing conditions. *Blood.* 100:4033–4039. doi:10.1182/blood-2002-05-1401

Doreian, B.W., T.G. Fulop, and C.B. Smith. 2008. Myosin II activation and actin reorganization regulate the mode of quantal exocytosis in mouse adrenal chromaffin cells. *J. Neurosci.* 28:4470–4478. doi:10.1523/JNEUROSCI.0008-08.2008

Erent, M., A. Meli, N. Moisoi, V. Babich, M.J. Hannah, P. Skehel, L. Knipe, G. Zupancic, D. Ogden, and T. Carter. 2007a. Rate, extent and concentration dependence of histamine-evoked Weibel-Palade body exocytosis determined from individual fusion events in human endothelial cells. *J. Physiol.* 583:195–212. doi:10.1113/jphysiol.2007.132993

Erent, M., A. Meli, N. Moisoi, V. Babich, M.J. Hannah, P. Skehel, L. Knipe, G. Zupancic, D. Ogden, and T.D. Carter. 2007b. Rate, extent and concentration dependence of histamine-evoked Weibel-Palade body exocytosis determined from individual fusion events in human endothelial cells. *J. Physiol.* 583:195–212. doi:10.1113/jphysiol.2007.132993

Gasman, S., S. Chasserot-Golaz, M. Malacombe, M. Way, and M.F. Bader. 2004. Regulated exocytosis in neuroendocrine cells: a role for subplasmalemmal Cdc42/N-WASP-induced actin filaments. *Mol. Biol. Cell.* 15:520–531. doi:10.1091/mbc.E03-06-0402

Guha, M., M. Zhou, and Y.L. Wang. 2005. Cortical actin turnover during cytokinesis requires myosin II. *Curr. Biol.* 15:732–736. doi:10.1016/j.cub.2005.03.042

Harrison-Lavoie, K.J., G. Michaux, L. Hewlett, J. Kaur, M.J. Hannah, W.W. Lui-Roberts, K.E. Norman, and D.F. Cutler. 2006. P-selectin and CD63 use different mechanisms for delivery to Weibel-Palade bodies. *Traffic*. 7:647–662. doi:10.1111/j.1600-0854.2006.00415.x

Hume, A.N., D.S. Ushakov, A.K. Tarafder, M.A. Ferenczi, and M.C. Seabra. 2007. Rab27a and MyoVa are the primary Mlph interactors regulating melanosome transport in melanocytes. *J. Cell Sci.* 120:3111–3122. doi:10.1242/jcs.010207

Larina, O., P. Bhat, J.A. Pickett, B.S. Launikonis, A. Shah, W.A. Kruger, J.M. Edwardson, and P. Thorn. 2007. Dynamic regulation of the large exocytotic fusion pore in pancreatic acinar cells. *Mol. Biol. Cell*. 18:3502–3511. doi:10.1091/mbc.E07-01-0024

Lui-Roberts, W.W., L.M. Collinson, L.J. Hewlett, G. Michaux, and D.F. Cutler. 2005. An AP-1/clathrin coat plays a novel and essential role in forming the Weibel-Palade bodies of endothelial cells. *J. Cell Biol.* 170:627–636. doi:10.1083/jcb.200503054

Manneville, J.B., S. Etienne-Manneville, P. Skehel, T. Carter, D. Ogden, and M. Ferenczi. 2003. Interaction of the actin cytoskeleton with microtubules regulates secretory organelle movement near the plasma membrane in human endothelial cells. *J. Cell Sci.* 116:3927–3938. doi:10.1242/jcs.00672

McEver, R.P., J.H. Beckstead, K.L. Moore, L. Marshall-Carlson, and D.F. Bainton. 1989. GMP-140, a platelet alpha-granule membrane protein, is also synthesized by vascular endothelial cells and is localized in Weibel-Palade bodies. *J. Clin. Invest.* 84:92–99. doi:10.1172/JCI114175

Medeiros, N.A., D.T. Burnette, and P. Forscher. 2006. Myosin II functions in actin-bundle turnover in neuronal growth cones. *Nat. Cell Biol.* 8:216–226. doi:10.1038/ncb1367

Metcalf, D.J., T.D. Nightingale, H.L. Zenner, W.W. Lui-Roberts, and D.F. Cutler. 2008. Formation and function of Weibel-Palade bodies. *J. Cell Sci.* 121:19–27. doi:10.1242/jcs.03494

Michaux, G., K.B. Abbitt, L.M. Collinson, S.L. Haberichter, K.E. Norman, and D.F. Cutler. 2006a. The physiological function of von Willebrand's factor depends on its tubular storage in endothelial Weibel-Palade bodies. *Dev. Cell*. 10:223–232. doi:10.1016/j.devcel.2005.12.012

Michaux, G., T.J. Pullen, S.L. Haberichter, and D.F. Cutler. 2006b. P-selectin binds to the D'-D3 domains of von Willebrand factor in Weibel-Palade bodies. *Blood*. 107:3922–3924. doi:10.1182/blood-2005-09-3635

Miklavc, P., O.H. Wittekindt, E. Felder, and P. Dietl. 2009. Ca2+-dependent actin coating of lamellar bodies after exocytotic fusion: a prerequisite for content release or kiss-and-run. *Ann. NY Acad. Sci.* 1152:43–52. doi:10.1111/j.1749-6632.2008.03989.x

Mitchell, T., A. Lo, M.R. Logan, P. Lacy, and G. Eitzen. 2008. Primary granule exocytosis in human neutrophils is regulated by Rac-dependent actin remodeling. *Am. J. Physiol. Cell Physiol.* 295:C1354–C1365. doi:10.1152/ajpcell.00239.2008

Mogilner, A., and G. Oster. 2003. Force generation by actin polymerization II: the elastic ratchet and tethered filaments. *Biophys. J.* 84:1591–1605. doi:10.1016/S0006-3495(03)74969-8

Murthy, K., and P. Wadsworth. 2005. Myosin-II-dependent localization and dynamics of F-actin during cytokinesis. *Curr. Biol.* 15:724–731. doi:10.1016/j.cub.2005.02.055

Nemoto, T., T. Kojima, A. Oshima, H. Bito, and H. Kasai. 2004. Stabilization of exocytosis by dynamic F-actin coating of zymogen granules in pancreatic acini. *J. Biol. Chem.* 279:37544–37550. doi:10.1074/jbc.M403976200

Nightingale, T.D., K. Pattni, A.N. Hume, M.C. Seabra, and D.F. Cutler. 2009. Rab27a and MyRIP regulate the amount and multimeric state of VWF released from endothelial cells. *Blood*. 113:5010–5018. doi:10.1182/blood-2008-09-181206

Riedl, J., A.H. Crevenna, K. Kessenbrock, J.H. Yu, D. Neukirchen, M. Bista, F. Bradke, D. Jenne, T.A. Holak, Z. Werb, et al. 2008. Lifeact: a versatile marker to visualize F-actin. *Nat. Methods*. 5:605–607. doi:10.1038/nmeth.1220

Romani de Wit, T., M.G. Rondaij, P.L. Hordijk, J. Voorberg, and J.A. van Mourik. 2003. Real-time imaging of the dynamics and secretory behavior of Weibel-Palade bodies. *Arterioscler. Thromb. Vasc. Biol.* 23:755–761. doi:10.1161/01.ATV.0000069847.72001.E8

Sadler, J.E. 2008. Von Willebrand factor, ADAMTS13, and thrombotic thrombocytopenic purpura. *Blood*. 112:11–18. doi:10.1182/blood-2008-02-078170

Sadler, J.E. 2009. von Willebrand factor assembly and secretion. *J. Thromb. Haemost.* 7(Suppl. 1):24–27. doi:10.1111/j.1538-7836.2009.03375.x

Sakamoto, T., J. Limouze, C.A. Combs, A.F. Straight, and J.R. Sellers. 2005. Blebbistatin, a myosin II inhibitor, is photoinactivated by blue light. *Biochemistry*. 44:584–588. doi:10.1021/bi0483357

Schietroma, C., H.Y. Yu, M.C. Wagner, J.A. Umbach, W.M. Bement, and C.B. Gundersen. 2007. A role for myosin 1e in cortical granule exocytosis in *Xenopus* oocytes. *J. Biol. Chem.* 282:29504–29513. doi:10.1074/jbc.M705825200

Segawa, A., and S. Yamashina. 1989. Roles of microfilaments in exocytosis: a new hypothesis. *Cell Struct. Funct.* 14:531–544. doi:10.1247/csf.14.531

Sokac, A.M., C. Co, J. Taunton, and W. Bement. 2003. Cdc42-dependent actin polymerization during compensatory endocytosis in *Xenopus* eggs. *Nat. Cell Biol.* 5:727–732. doi:10.1038/ncb1025

Sokac, A.M., C. Schietroma, C.B. Gundersen, and W.M. Bement. 2006. Myosin-1c couples assembling actin to membranes to drive compensatory endocytosis. *Dev. Cell*. 11:629–640. doi:10.1016/j.devcel.2006.09.002

Straight, A.F., A. Cheung, J. Limouze, I. Chen, N.J. Westwood, J.R. Sellers, and T.J. Mitchison. 2003. Dissecting temporal and spatial control of cytokinesis with a myosin II Inhibitor. *Science*. 299:1743–1747. doi:10.1126/science.1081412

Trifaró, J.M., S. Gasman, and L.M. Gutiérrez. 2008. Cytoskeletal control of vesicle transport and exocytosis in chromaffin cells. *Acta Physiol. (Oxf.)*. 192:165–172. doi:10.1111/j.1748-1716.2007.01808.x

Valentijn, J.A., L.T. Gien, K.M. Valentijn, and J.D. Jamieson. 2000a. An evaluation of the expression, subcellular localization, and function of rab4 in the exocrine pancreas. *Biochem. Biophys. Res. Commun.* 268:847–852. doi:10.1006/bbrc.2000.2221

Valentijn, J.A., K. Valentijn, L.M. Pastore, and J.D. Jamieson. 2000b. Actin coating of secretory granules during regulated exocytosis correlates with the release of rab3D. *Proc. Natl. Acad. Sci. USA*. 97:1091–1095. doi:10.1073/pnas.97.3.1091

Vallotton, P., S.L. Gupton, C.M. Waterman-Storer, and G. Danuser. 2004. Simultaneous mapping of filamentous actin flow and turnover in migrating cells by quantitative fluorescent speckle microscopy. *Proc. Natl. Acad. Sci. USA*. 101:9660–9665. doi:10.1073/pnas.0300552101

Wagner, D.D. 1990. Cell biology of von Willebrand factor. *Annu. Rev. Cell Biol.* 6:217–246. doi:10.1146/annurev.cb.06.110190.001245

Wagner, D.D., S. Saffaripour, R. Bonfanti, J.E. Sadler, E.M. Cramer, B. Chapman, and T.N. Mayadas. 1991. Induction of specific storage organelles by von Willebrand factor propolypeptide. *Cell*. 64:403–413. doi:10.1016/0092-8674(91)90648-I

Waselle, L., T. Coppola, M. Fukuda, M. Iezzi, A. El-Amraoui, C. Petit, and R. Regazzi. 2003. Involvement of the Rab27 binding protein Slac2c/MyRIP in insulin exocytosis. *Mol. Biol. Cell*. 14:4103–4113. doi:10.1091/mbc.E03-01-0022

Weibel, E.R., and G.E. Palade. 1964. New cytoplasmic components in arterial endothelia. *J. Cell Biol.* 23:101–112. doi:10.1083/jcb.23.1.101

Wilson, C.A., M.A. Tsuchida, G.M. Allen, E.L. Barnhart, K.T. Applegate, P.T. Yam, L. Ji, K. Keren, G. Danuser, and J.A. Theriot. 2010. Myosin II contributes to cell-scale actin network treadmilling through network disassembly. *Nature*. 465:373–377. doi:10.1038/nature08994

Yu, H.Y., and W.M. Bement. 2007. Multiple myosins are required to coordinate actin assembly with coat compression during compensatory endocytosis. *Mol. Biol. Cell*. 18:4096–4105. doi:10.1091/mbc.E06-11-0993